

## Wake Capture, Particle Breakup and Other Artifacts Associated with Counterflow Virtual Impaction

Mikhail S. Pekour<sup>1</sup> and Daniel J. Cziczo<sup>1,2,\*</sup>

<sup>1</sup>Atmospheric Science and Global Change Division, Pacific Northwest National Laboratory, 902 Battelle Blvd., Richland, Washington, USA.

<sup>2</sup>Now at: Department of Earth, Atmosphere, and Planetary Sciences, Massachusetts Institute of Technology, Cambridge, Massachusetts, USA.

\*Corresponding author. E-mail: [djcziczo@mit.edu](mailto:djcziczo@mit.edu)

### Abstract

Counterflow virtual impaction is used to inertially separate cloud elements from un-activated aerosol. Previous airborne, ground-based and laboratory studies using this technique exhibit artifacts that are not fully explained by impaction theory. We have performed laboratory studies that show small particles can be carried across the inertial barrier of the counterflow by collision and/or coalescence or riding the wake of larger particles with sufficient inertia. We have also performed theoretical calculations to show that aerodynamic forces associated with the requisite acceleration and deceleration of particles within a counterflow virtual impactor can lead to breakup. The implication of these processes on studies using this technique are discussed.

### Introduction

The counterflow virtual impactor (CVI) was developed as a means to separate cloud elements from un-activated aerosol so that the former can be analyzed (Ogren 1985). Particles are drawn into a CVI due to the motion of an aircraft (Laucks and Twohy 1998), the velocity imparted by a wind tunnel (Noone et al. 1998) or a vacuum pump (Boulter et al. 2006). The later variant is termed a pumped CVI (PCVI).

Counterflow virtual impaction, despite its numerous uses and advantages, is subject to artifacts. These include particles transmitted by the CVI that are (1) more numerous than the number of cloud elements (Schwarzenböck and Heintzenberg 2000), (2) chemically were unlikely to form the cloud elements (DeMott et al. 2004), and (3) smaller than the cut-size (Kulkarni et al. 2010). Some of these phenomena can be explained by cloud element impaction on surfaces which liberates previously deposited aerosol and/or results in surface pitting (Murphy et al. 2004). Schwarzenböck and Heintzenberg (2000) described another source of artifacts, the process of droplet breakup when aerodynamic stress exceeds the surface tension.

Here we show that particles larger than the cut-size of a CVI facilitate the transmission of smaller particles. Processes such as collision and coalescence, collision resulting in kinetic energy increase, and wake capture are possible explanations. In the absence of particles larger

than the cut-size, experiments show that the CVI rejects essentially all smaller particles. To our knowledge this phenomena has not been previously described or considered as a source of artifacts. In addition, we use a theoretical model to show that acceleration and deceleration forces within a CVI can exceed cohesive forces of droplets and ice crystals thereby leading to breakup. Because the location of breakup is dependent on particle size and phase both rejection of cloud elements that should have been transmitted and retention of multiple fragments can result.

## Experiments and Results

The experiments described here were conducted on a PCVI described in the literature (Boulter et al. 2006; Kulkarni et al. 2010). Note that Boulter et al. dealt mainly with an initial description of the PCVI design whereas Kulkarni et al. dealt with non-ideal behavior explained through computational fluid dynamic modeling. A schematic of the PCVI with a definition of flows and other terms used in the text is shown in Figure 1. Polystyrene latex (PSL) spheres (Thermo Scientific, Fremont, CA) were atomized (TSI Model 3076, Shoreview, MN or Salter Lab 8900 Series Jet Nebulizer, Arvin, CA) from distilled, deionized water. In cases where two sizes of spheres were investigated two identical nebulizers were used. Particle number and size were measured using an Aerodynamic Particle Sizer (APS, TSI Model 3021, Shoreview, MN) and/or a Laser Aerosol Spectrometer (LAS, Model 3340, Shoreview, MN). Figure 2 shows the size-resolved number density of 1.0 micrometer diameter PSLs before (a) and after the PCVI. Panels (b)-(d) show cases where the counterflow was varied to create a cut-size of 2.9, 3.2, and 3.5 micrometers diameter. Note that essentially none of the particles are transmitted in these cases. Particle number density before the PCVI for a dual atomization of 1.0 and 5.0 micrometer PSLs is shown in panel (e). The same counterflow rates as in panels (b)-(d) were then applied for panels (f)-(h), respectively. In the presence of particles larger than the cut-size smaller particles were unintentionally transmitted.

Figure 1

Figure 2

Experiments were performed for a variety of large and small particle sizes and number densities. The small particle sizes utilized were 0.22, 0.45, 0.90 and 1.0 micrometers diameter. Concentration was constant for a single experiment but were varied over an order of magnitude (from 30 to 300 per cubic centimeter) between experiments. Large particle sizes utilized were 3.0, 5.0 and 5.5 micrometers diameter with concentration ranging from 0.25 to 10 per cubic centimeter. All experiments were performed at laboratory conditions (i.e., no temperature, humidity, or pressure control was employed). The experimental temperature range was 18—23 °C, the ambient humidity was 30—36% and the PCVI pressure was 86—87 kPa with atmospheric pressure 101 kPa. Only in cases where particles larger than the cut-size were present were small particles observed to be unintentionally transmitted. Figure 3 shows experimental data of the ratio of the number density of small transmitted particles ( $n_{out}$ ) versus the product of

the initial small and transmitted large particle number density ( $n_{in}$  and  $N_{out}$ , respectively) to the counterflow rate. This ratio is used to normalize the unintentionally transmitted particles to their initial abundance and the number of large particles which appear to facilitate their transmission. The abscissa in 3 is the counterflow rate which determines the amount of time a particle smaller than the cut-size is present between the two stagnation planes (see Boulter et al. 2006 and Kulkarni et al. 2010 for specific details); counterflow is therefore inversely proportional to the amount of time large and small particles interact. Note that this statement is not true of all CVIs; those which utilize a porous frit for introduction of the counterflow have as a result a variable length region of interaction (e.g., Laucks and Twohy et al. 1998). Lower unintentionally transmitted numbers are observed as counterflow is increased (i.e., as interaction time is decreased). In all cases in Figure 3 the counterflow is sufficient to allow transmission of the larger particles but should reject the smaller ones.

Figure 3

We propose three possible explanations that are consistent with the data:

- (1) Small particles between the stagnation planes are struck by large particles in a quasi-elastic “billiard ball” collision which imparts sufficient kinetic energy to allow them to cross into the sample flow.
- (2) Small particles become entrained in the wake of the large particles and are carried into the sample. Note that the wake of a large particle in a CVI is complex and switches direction as it crosses the stagnation planes.
- (3) Small particles are collected via collision and coalescence with the large particles. Small particles would then need be ‘detained’ in the sample flow.

Geometric estimates of collision and assuming unit coalescence were performed and show that ~30 % of the unintentionally transmitted particles can be ascribed to (1) and (3). Note that the geometric approach, where the effective collection size of the large particle is set to its physical size, does not address wake capture. Table 1 provides values for the Reynolds Number for particles in the PCVI according to Hinds (1999). Flow eddies will develop in a particle wake for values  $> 1$  which is the case for all super-micrometer diameter particles.

Table 1

Figure 3 shows that the larger the size of the large particle the more abundant the unintentionally transmitted small particles; this behavior is consistent with these three possible explanations. Larger small particles generally tend to lead to larger unintentional transmission although data exhibit scatter. Increased transmission of larger small particles would tend to favor the “billiard ball” and “collision and coalescence” mechanisms although larger particles also have a longer time for interaction in the region between the two stagnation planes regardless of the mechanism.

It is possible all three mechanisms are important and we can not preclude that any of them dominates depending on the specific particle sizes, number densities and flow conditions.

In order to understand interaction time between the stagnation planes the gas and size-dependent particle velocity on the center line as a function of distance through the PCVI are shown in Figure 4. A cross-section of the PCVI is shown in the lower panel of Figure 4 for reference. Figure 1 gives a more comprehensive picture with the orifice where the input flow is accelerated, the pump port where gas and small particles are removed, the counterflow port, and the output orifice are denoted in the caption. A gas velocity profile was calculated where the cross-section of the channel changed with velocities linearly interpolated between profiles. The flow was assumed to be turbulent, viscous, and incompressible. Profiles were calculated either using a turbulent velocity deficit profile (Kay and Nedderman, 1974) or following Barenblatt et al. (1997). Particle velocities were estimated following a kinetic energy change approach: particles were assumed to be in equilibrium with the gas flow at the PCVI entrance. Subsequent gas velocity changes resulted in a particle-gas velocity difference and a resulting drag force which lead to a change in particle kinetic energy. For each step along the PCVI channel this change was expressed as:

$$\frac{m_p v_i^2}{2} = \frac{m_p v_{i-1}^2}{2} + \Delta x \cdot F_D(D_p, v_i - V_i, Re_p, C_p) \quad (1)$$

where  $m_p$  is particle mass,  $v$  is particle velocity,  $V$  is local gas velocity,  $\Delta x$  is a step along the PCVI channel,  $F_D$  is drag force which depends on particle diameter  $D_p$ , particle-gas velocity difference  $v-V$ , particle Reynolds number  $Re_p$ , and slip correction factor  $C_p$ .  $F_d$  was estimated following Hinds (1999) and Baron and Willeke (2005). Particles which reached a velocity of zero were assumed removed from the system (i.e., removed by the pump flow). Calculations were performed for traces at different radii from the center line and for a range of particle sizes in order to resolve the transmission curve. Very small particles essentially follow the gas streamlines and are removed from the system at the 1<sup>st</sup> stagnation plane (the left-most dashed line). Small particles just below the cut-size are only stopped and turned around at the 2<sup>nd</sup> stagnation plane (the right-most dashed line); such particles therefore spend a considerable time in the interaction region first moving up to the 2<sup>nd</sup> stagnation plane before pausing and then being moved back to the pump flow.

Figure 4

Figure 4 also shows that particles larger than the cut-size are first accelerated in the input orifice before being decelerated by the counterflow. Acceleration and deceleration place an aerodynamic stress on the particle which can exceed the material cohesion or make a liquid particle dynamically unstable. In the case of water droplets breakup is normally indicated by the Weber number:

$$We = (V-v)^2 \rho_p D_p / \gamma \quad (2)$$

where  $\rho_p$  is the droplet density and  $\gamma$  is the droplet surface tension. The literature suggests values of  $We$  between 5 and 20 as the limit to initiate breakup (Schwarzenbock and Heintzenger 2000; Baron and Willeke 2001; Twohy et al. 2003; Kolev 2007; Vidaurre and Hallett 2009). Based on the velocity differential shown in Figure 4 calculations of Weber number are given in Table 1 for droplet sizes from 0.5 to 75 micrometers. Note that particles larger than 25 micrometers have  $We > 10$  in the acceleration region of the orifice and particles larger than 75 micrometers exceed this value in the deceleration region.

The process of ice breakup is more complicated since crystals have variable density and morphology and features such as structural defects may facilitate fracturing. Only limited information on the physical properties of atmospheric ice is available. Tensile or compressive strength estimates vary by five orders of magnitude: Supulver et al. (1997) mentions 10-100 Pa for comet ice and 200-2500 Pa for water frost, Bacon et al. (1998) found  $10^4 - 4 \times 10^4$  Pa for levitated frost particles and  $10^6$  Pa is often used for solid bulk ice (Schulson 1999). Table 2 is analogous to Table 1 but for estimation of the aerodynamic stress ( $St$ ) on ice for variable size and material density:

$$St = \rho_a (V-v)^2 / 2 \quad (3)$$

where  $\rho_a$  is the air density. Note that there is a local maximum in stress as a function of particle size due to size-dependent acceleration. Note that given the uncertainty in tensile strength it is currently not possible to determine if or where ice may break up within a CVI; experiments are required to reduce the bounds given above in order to make progress in this area.

Table 2

## Conclusions and Implications

Experimental results show that particles above the cut-size of a CVI can facilitate the transmission of particles that should be inertially rejected. There does not appear to be a simple means of eliminating this artifact. For a scenario where there are 100 droplets and 1000 unactivated aerosols per cc we estimate that up to 1% of transmitted particles may be an artifact. This is one example and the exact level of unintentional transmission is a function of the large and small particle number densities and sizes as well as the flow conditions in the instrument that is used. The relative abundance of this artifact will therefore be dependent on the specific CVI and experimental conditions and should be quantified on a case by case basis.

A simple theoretical model was also used to consider the breakup of droplets and ice crystals within a CVI by comparing aerodynamic conditions to material cohesion and droplet stability. Both the acceleration force found in the inlet and the deceleration force in the counterflow region were observed to be capable of inducing droplet or ice breakup. These two breakup locations can have very different effects on sampling. Breakup in the acceleration region can lead to fragments smaller than the cut-size and rejection of a particle that should be transmitted. Fragmentation in the deceleration region conversely results in multiple particles transmitted from a single cloud element. It is noteworthy that the fragmentation process for ice is less well understood than for liquid water due to uncertainty in density and material properties; we recommend that

experiments be conducted in order to better understand this phenomena. We also note that with careful design of a CVI acceleration forces in these regions could be lowered.

For these reasons it is unclear if and when particles can be counted after a CVI and compared to the ambient abundance of cloud elements. In some cases CVI artifacts may be small when compared to uncertainty in other quantities or the detection limits of downstream analytical techniques. None the less, the aforementioned artifacts can lead to cases where more or less particles than should be are transmitted. The veracity of downstream analyses must be considered, especially in the case of unintentional transmission where non-cloud elements are entrained in the sample flow with cloud element residuals.

Measurements of condensed-phase water are probably correct since little water is carried by small, unintentionally transmitted particles and breakup in the counterflow region does not add or subtract water from the system. One exception is a case with inlet acceleration forces (e.g., in a wind tunnel or PCVI) and large cloud elements which can be fragmented and rejected are present, thereby leading to an underestimation of condensed-phase water. A measurement strategy that should not be significantly affected by artifacts is the separation of cloud elements and subsequent re-activation using a cloud chamber (e.g., Prenni et al. 2007). In this case the incorrectly transmitted aerosol or fragments are not re-activated within the cloud chamber and the determined number density should be comparable to cloud element abundance.

### **Acknowledgements**

Funding for this work was provided by the Pacific Northwest National Laboratory Aerosol and Climate Initiative. The authors wish to thank Gourihar Kulkarni for useful discussions.

**Table 1.** Velocity difference between gas and particles and resultant Weber and Reynolds numbers as a function of particle size in the input (acceleration) and stagnation (deceleration) regions (see Equation 2 and Figure 1). Droplet breakup is suggested for Weber numbers greater than 10, denoted in bold in the table. Wake eddies develop for Reynolds numbers great than 1 (Hinds 1999). See text for details.

**Table 2.** Aerodynamic stress resulting from the velocity difference between particle and gas phases in the input (acceleration) and stagnation (deceleration) regions as a function of particle diameter for three different values of ice density (see Equation 3). See text for details.

**Figure 1.** Cross sectional schematic of the pumped counterflow virtual impactor used in these studies. Incoming particles and gas are accelerated as they pass two reducing orifices (distance = 0 and 32.5 mm, respectively). Gas and small particles are pumped away before reaching the 1<sup>st</sup> stagnation plane (left-most dashed line, distance ~ 35 mm) whereas particles just below the inertial threshold penetrate to the 2<sup>nd</sup> stagnation plane (right-most dashed line, distance ~ 36 mm) where they are stopped and turned around. Large particles pass both stagnation planes but are decelerated and then slightly re-accelerated as they enter the sample flow. Flow names are given in the figure as well as the location of interaction zones described in the text.

**Figure 2.** Size-resolved particle density as a function of experimental conditions. Particles produced from atomized 1 micrometer diameter PSL solution for a measurement made at the PCVI input (a). Particles smaller than 1.0 micrometer are due to the organic matrix in which PSLs are delivered. Panels (b)-(d) are the number densities after the PCVI for a cut-size of 2.9, 3.2, and 3.5 micrometers diameter. Panel (e), analogous to (a), is the particle density produced before the PCVI from an atomized PSL solution with both 1 and 5 micrometer particles. Panels (f)-(g) are the densities after the PCVI for the same counterflow as in (b)-(d), which should be sufficient to reject 1.0 while transmitting 5.0 micrometer particles. Note ‘breakthrough’ of some 1.0 micrometer PSLs. Each panel represents 5 minutes of data. Number of particles above ( $N$ ) and below ( $n$ ) the cut-size during each sample period is given in the panels.

**Figure 3.** Ratio of the number of particles below the cut-size that are transmitted ( $n_{out}$ ) to the initial number of small ( $n_{in}$ ) and large transmitted ( $N_{out}$ ) particles as a function of the counterflow. The diameter of the small and large particles for each curve is given in the legend.

**Figure 4.** Gas (solid blue) and particle (red lines according to size in legend) velocity as a function of distance along the length on the center line of a PCVI. The PCVI profile, repeated from Figure 1, is shown in the lower panel. Thick black lines denote regions where droplets may breakup (see Table 1). See text for details.

## References

- Bacon, N. J., Swanson, B. D., and Baker, M. B. (1998). Breakup of Levitated Frost Particles, *J. Geophys. Res.*, 103: 13763-13775.
- Barenblatt, G. I., Chorin, A. J. and Prostokishin, V. M. (1997). Scaling Laws for Fully Developed Turbulent Flow in Pipes, *Appl. Mech. Rev.* 50: 413-423.
- Baron, P. A., and Willeke, K. (2001). *Aerosol Measurement: Principles, Techniques and Applications*, 2<sup>nd</sup> Edition, Wiley-Interscience, New York, pp. 69-71.
- Boulter, J. E., Cziczo, D. J., Middlebrook, A. M., Thomson, D. S., and Murphy, D. M. (2006). Design and Performance of a Pumped Counterflow Virtual Impactor, *Aerosol Sci. Technol.*, 40: 969-976.
- DeMott, P. J., Cziczo, D. J., Prenni, A. J., Murphy, D. M., Kreidenweis, S. M., Thomson, D. S., Borys, R., and Rogers, D. C. (2003). Measurements of the concentration and composition of nuclei for cirrus formation, *PNAS*, 100: 14655-14660.
- Hinds, W. C. (1999). *Aerosol Technology: Properties, Behavior, and Measurement of Airborne Particles*, 2<sup>nd</sup> Edition, Wiley-Interscience, New York, pp. 230-254.
- Kay, J. M., and Nedderman, R. M. (1974). *An Introduction to Fluid Mechanics and Heat Transfer: With Applications in Chemical & Mechanical Process Engineering*, Cambridge University Press, Cambridge, UK, pp. 32-33.
- Kolev, N. I. (2007). *Multiphase Flow Dynamics: Thermal and Mechanical Interactions*, Springer, New York, p. 207.
- Kulkarni, G., Pekour, M., Afchine, A., Murphy, D. M., and Cziczo, D. J. (2011). Comparison of Experimental and Numerical Studies of the Performance Characteristics of a Pumped Counterflow Virtual Impactor, *Aerosol Sci. Technol.*, 45, 382-392.
- Laucks, M. L., and Twohy, C. H. (1998). Size-dependent Collection Efficiency of an Airborne Counterflow Virtual Impactor, *Aerosol Sci. Technol.* 28: 40-61.
- Murphy, D.M., Cziczo, D.J., Hudson, P.K., Thomson, D.S., Wilson, J.C., Kojima, T. and Buseck, P.R. (2004). Particle Generation and Resuspension in Aircraft Inlets When Flying in Clouds, *Aerosol Sci. Technol.* 38: 400-408.



Noone, K. J., Ogren, J. A., Heintzenberg, J., Charlson, R. J., and Covert, D. S. (1988). Design and Calibration of a Counterflow Virtual Impactor for Sampling of Atmospheric Fog and Cloud Droplets, *Aerosol Sci. Technol.* 8: 235–244.

Ogren, J. A., Heintzenberg, J., and Charlson, R. J. (1985). In-situ Sampling of Clouds With a Droplet to Aerosol Converter, *Geophys. Res. Lett.* 12: 121–124.

Prenni, A. J., DeMott, P. J., Twohy, C., Poellot, M. R., Kreidenweis, S. M., Rogers, D. C., Brooks, S. D., Richardson, M. S. and Heymsfield, A. J. (2007). Examinations of Ice Formation Processes in Florida Cumuli Using Ice Nuclei Measurements of Anvil Ice Crystal Particle Residues, *J. Geophys. Res.* 112: 1-16.

Schwarzenböck, A. and Heintzenberg, J. (2000). Cut Size Minimization and Cloud Element Break-up in a Ground Based CVI, *J. Aerosol Sci.* 31: 477-489.

Schulson, E. M. (1999). The Structure and Mechanical Behavior of Ice, *JOM* 51: 21-27.

Supulver, K. D., Bridges, F. G., Tiscareno, S. and Lievore, J. (1997). The Sticking Properties of Water Frost Produced under Various Ambient Conditions, *ICARUS* 129: 539-554.

Twohy, C. H., Strapp, J. W., and Wendisch, M. (2003). Performance of a Counterflow Virtual Impactor in the NASA Icing Research Tunnel, *J. Atmos. Ocean. Tech.* 20: 781-790.

Vidaurre, G. and Hallett, J. (2009). Particle Impact and Breakup in Aircraft Measurements, *J. Atmos. Ocean. Tech.* 26: 972-983.

Diameter [ $\mu\text{m}$ ]	Input Region			Stagnation Region		
	Velocity difference [m/s]	Weber number	Reynolds number	Velocity difference [m/s]	Weber number	Reynolds number
0.5	-44.13	0.02	1	28.98	0.01	1
1	-74.6	0.09	5	71.23	0.08	5
5	-120.14	1.25	42	149.98	2.02	54
10	-128.97	3.12	96	135.54	3.49	103
25	-146.32	<b>12.54</b>	341	110.4	6.29	227
50	-160.1	<b>39.43</b>	981	94.1	9.89	419
75	-166.84	<b>77.46</b>	1850	86.39	<b>13.26</b>	613

Ice density:  
260[kg/m<sup>3</sup>]

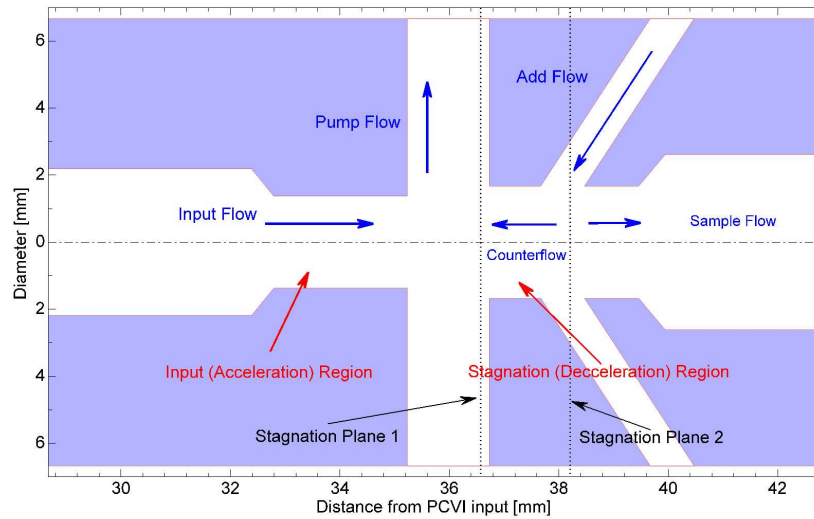
D [μm]	$\Delta V_{in}$ [m/s]	$\Delta V_{stag}$ [m/s]	Stress <sub>in</sub> [Pa]	Stress <sub>stag</sub> [Pa]
1	-54	43	316	424
3	-100	127	2858	1415
5	-114	161	4578	1846
10	-125	164	4781	2213
15	-130	154	4214	2382
22	-136	143	3599	2601
50	-153	117	2407	3278
75	-160	106	1974	3616
100	-165	99	1738	3826

Ice density:  
500[kg/m<sup>3</sup>]

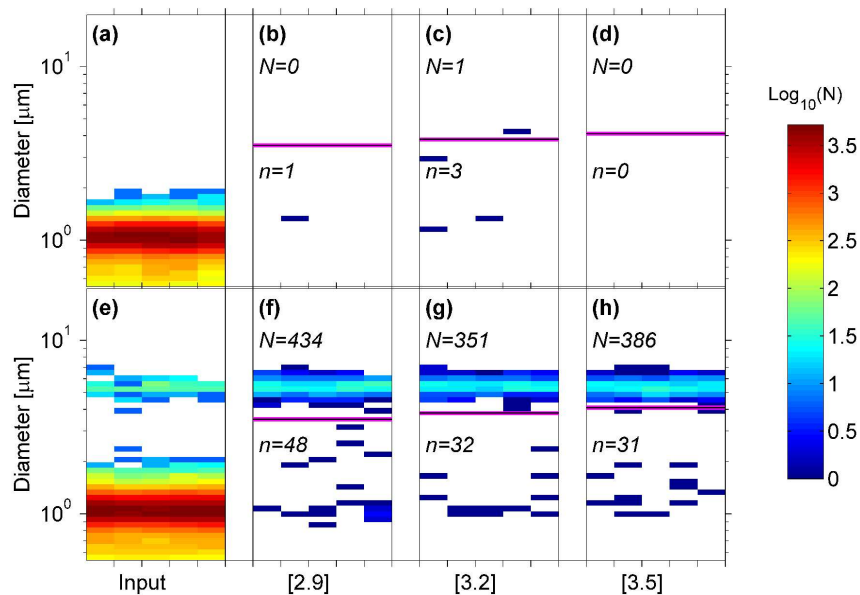
D [μm]	$\Delta V_{in}$ [m/s]	$\Delta V_{stag}$ [m/s]	Stress <sub>in</sub> [Pa]	Stress <sub>stag</sub> [Pa]
1	-73	73	927	766
3	-112	156	4340	1766
5	-122	169	5035	2087
10	-130	154	4223	2370
15	-136	142	3556	2604
22	-144	129	2954	2904
50	-161	105	1946	3630
75	-167	96	1631	3919
100	-170	91	1471	4079

Ice density:  
917[kg/m<sup>3</sup>]

D [μm]	$\Delta V_{in}$ [m/s]	$\Delta V_{stag}$ [m/s]	Stress <sub>in</sub> [Pa]	Stress <sub>stag</sub> [Pa]
1	-90	107	2043	1144
3	-120	169	5037	2015
5	-126	163	4727	2238
10	-135	143	3609	2569
15	-143	129	2961	2884
22	-152	117	2420	3238
50	-167	96	1632	3912
75	-171	89	1415	4133
100	-174	86	1311	4244

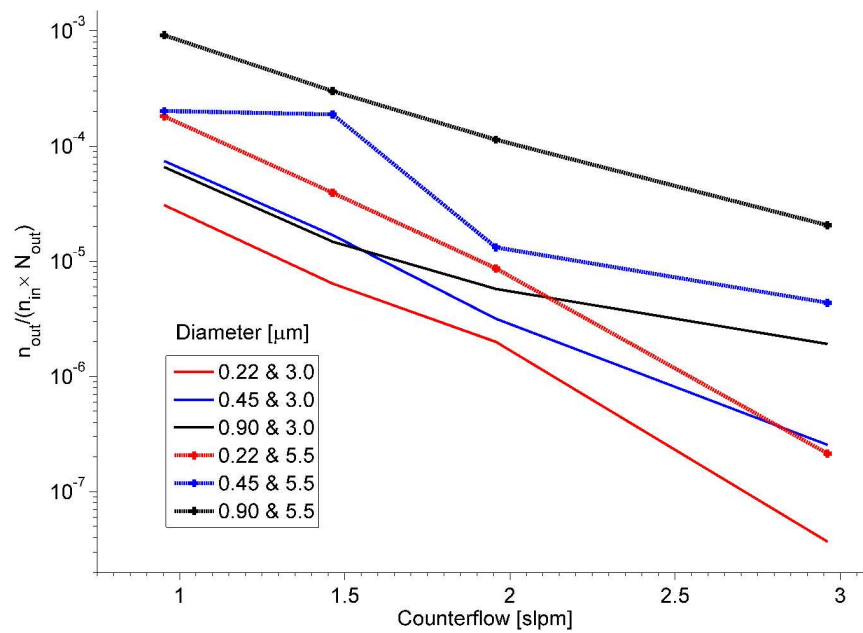


Cross sectional schematic of the pumped counterflow virtual impactor used in these studies. Incoming particles and gas are accelerated as they pass two reducing orifices (distance = 0 and 32.5 mm, respectively). Gas and small particles are pumped away before reaching the 1st stagnation plane (left-most dashed line, distance ~ 35 mm) whereas particles just below the inertial threshold penetrate to the 2nd stagnation plane (right-most dashed line, distance ~ 36 mm) where they are stopped and turned around. Large particles pass both stagnation planes but are decelerated and then slightly re-accelerated as they enter the sample flow. Flow names are given in the figure as well as the location of interaction zones described in the text.  
329x189mm (600 x 600 DPI)

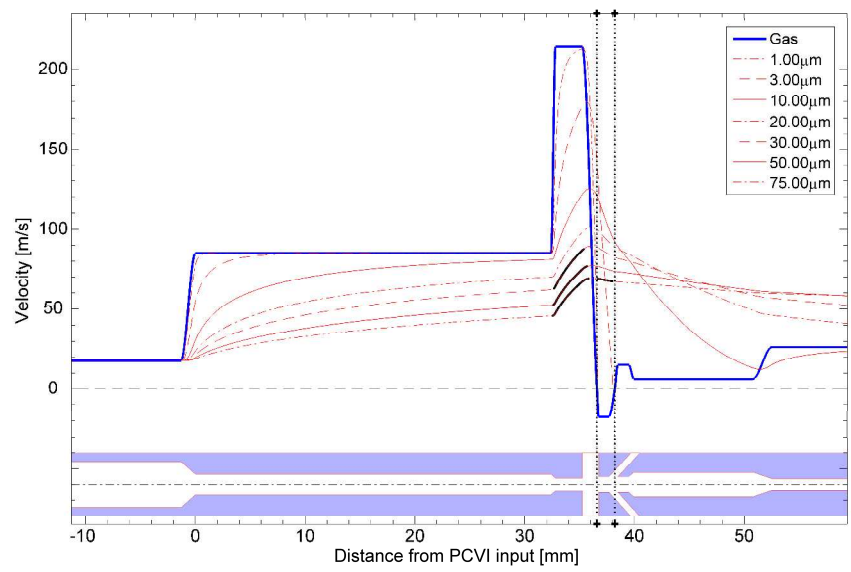


Size-resolved particle density as a function of experimental conditions. Particles produced from atomized 1 micrometer diameter PSL solution for a measurement made at the PCVI input (a). Particles smaller than 1.0 micrometer are due to the organic matrix in which PSLs are delivered. Panels (b)-(d) are the number densities after the PCVI for a cut-size of 2.9, 3.2, and 3.5 micrometers diameter. Panel (e), analogous to (a), is the particle density produced before the PCVI from an atomized PSL solution with both 1 and 5 micrometer particles. Panels (f)-(g) are the densities after the PCVI for the same counterflow as in (b)-(d), which should be sufficient to reject 1.0 while transmitting 5.0 micrometer particles. Note 'breakthrough' of some 1.0 micrometer PSLs. Each panel represents 5 minutes of data. Number of particles above ( $N$ ) and below ( $n$ ) the cut-size during each sample period is given in the panels.

261x174mm (600 x 600 DPI)



Ratio of the number of particles below the cut-size that are transmitted ( $n_{out}$ ) to the initial number of small ( $n_{in}$ ) and large transmitted ( $N_{out}$ ) particles as a function of the counterflow. The diameter of the small and large particles for each curve is given in the legend.  
266x183mm (600 x 600 DPI)



Gas (solid blue) and particle (red lines according to size in legend) velocity as a function of distance along the length on the center line of a PCVI. The PCVI profile, repeated from Figure 1, is shown in the lower panel. Thick black lines denote regions where droplets may breakup (see Table 1). See text for details.

316x198mm (600 x 600 DPI)